Water-Air Exchanges In The Lower Estuary Of The Patos Lagoon: Seasonal Variability, Drivers, And Sources Of CO2

Cíntia Albuquerque (cintia_albuquerque@furg.br)
Instituto de Oceanografia, Universidade Federal do Rio Grande - FURG https://orcid.org/0000-0002-3185-328X

Rodrigo Kerr
Instituto de Oceanografia, Universidade Federal do Rio Grande - FURG

Thiago Monteiro
Instituto de Oceanografia, Universidade Federal do Rio Grande - FURG

Eunice da Costa Machado
Universidade Federal do Rio Grande - FURG, Av. Itália km 8 s/n

Andréa da Consolação de Oliveira Carvalho
Instituto de Oceanografia, Universidade Federal do Rio Grande - FURG

Carlos Rafael Borges Mendes
Instituto de Oceanografia, Universidade Federal do Rio Grande - FURG

Research Article

Keywords: estuaries, carbon dioxide, CO2 partial pressure, CO2 fluxes

Posted Date: February 10th, 2022

DOI: https://doi.org/10.21203/rs.3.rs-1336400/v1

Water-air exchanges in the lower estuary of the Patos Lagoon: seasonal variability, drivers, and sources of CO_2

Cíntia Albuquerque[1,2,3,*], Rodrigo Kerr[1,2,3,*], Thiago Monteiro[1,2,3], Eunice da Costa Machado[3,4], Andréa da Consolação de Oliveira Carvalho[1,2,3], Carlos Rafael B. Mendes[1,5]

[1] Laboratório de Estudos dos Oceanos e Clima – LEOC, Instituto de Oceanografia, Universidade Federal do Rio Grande - FURG, Av. Itália km 8 s/n, Campus Carreiros, Rio Grande, RS, 96203-900, Brazil.

[2] Brazilian Ocean Acidification Network – BrOA, Av. Itália km 8, Rio Grande, 96203-900, RS, Brazil.

[3] Programa de Pós-Graduação em Oceanologia – PPGO, Instituto de Oceanografia, Universidade Federal do Rio Grande - FURG, Av. Itália km 8 s/n, Campus Carreiros, Rio Grande, RS, 96203-900, Brazil.

[4] Laboratório de Hidroquímica, Instituto de Oceanografia, Universidade Federal do Rio Grande - FURG, Av. Itália km 8 s/n, Campus Carreiros, Rio Grande, RS, 96203-900, Brazil.

[5] Laboratório de Fitoplâncton e Micro-organismos Marinhos, Instituto de Oceanografia, Universidade Federal do Rio Grande - FURG, Av. Itália km 8 s/n, Campus Carreiros, Rio Grande, RS, 96203-900, Brazil.

* Corresponding authors:

Address: CEOCEAN, LEOC, Instituto de Oceanografia, Universidade Federal do Rio Grande – FURG, Av. Itália km 8 s/n, Campus Carreiros, Rio Grande, RS, 96203-900, Brazil.
E-mails: cintia_albuquerque@furg.br, rodrigokerr@furg.br

Highlights

- The lower zone of the Patos Lagoon Estuary (PLE) is an annual net CO_2 sink zone.
- The CO_2 uptake in the PLE surface waters during the summer/autumn seasons is nearly twofold higher than the winter/spring CO_2 emissions.
- Autochthonous CO_2 production dominates the carbon dynamics in the PLE.
- The high surface water dynamics in the mouth of the PLE prevent accumulation of CO_2 and enable carbon export to the adjacent coast.

Submitted to Biogeochemistry

Acknowledgments

This study contributes to the activities of the Brazilian Ocean Acidification Network (BrOA; www.broa.furg.br) and the CARBON-FLUX project (National Council for Scientific and Technological Development – CNPq grant no. 420118/2018–7). C.A.W.C. received PhD. grant no. 88887.478990/2020–00 from the Coordination for the Improvement of Higher Education Personnel (CAPES). R.K. and C.R.B. received researcher grant nos. 304937/2018–5 and 306899/2018–3 from CNPq, respectively. We acknowledge the availability of the monitoring database provided by the Patos Lagoon Brazilian Long-Term Ecological Research Program (database available at https://doi.org/10.15468/xmlvxm), which has received grants from CNPq no. 441492/2016–9, FAPERGS no. 16/2551–0000102–2, and CAPES no. 16/2551–0000102–1. The BrOA Network dataset is available by request (https://carbonteam.furg.br/2-uncategorized/47-monitoramento). We also acknowledge the resources provided by CAPES to support the Graduate Program in Oceanology and free access to many scientific journals through *Periódicos* CAPES. We thank all the researchers, technicians and students who have been involved with and contributed to fostering this valuable database on the PLE.

Author contributions

C.A. conducted the data analysis and main interpretations of this study as part of her Ph.D thesis. R.K. lead the BrOA activities in the Patos Lagoon, proposed the study and supervised C.A. in conducting the planning and data collection in this study. E.M., T.M., and A.C.O.C contributed as experts in carbonate system and biogeochemical processes. C.R.B.M. contributed as an expert on phytoplankton and ecology. All authors contributed to the interpretation of results and writing the manuscript as experts on CO_2 systems.

Abstract

We investigated the primary drivers of changes in the partial pressure of carbon dioxide (pCO_2) together with the seasonal and interannual variability in the water-air net carbon dioxide flux (FCO_2) in the lower estuarine zone surface waters of Patos Lagoon, the largest choked lagoon worldwide. Sampling occurred monthly during May 2017-June 2021 at the estuary's inner inlet and mouth, which are contrasting hydrodynamic zones in the Patos Lagoon Estuary (PLE). The water pCO_2 was mainly controlled by seasonal changes in total alkalinity and total dissolved inorganic carbon. The lower zone experienced periods of CO_2 ingassing (austral summer/autumn) and CO_2 outgassing (austral winter/spring). During summer/autumn, both protected and sea-exposed areas uptake an average of –15 mmol m^{-2} d^{-1} CO_2, whereas during winter/spring, CO_2 emissions prevail, reaching an average of 22 mmol m^{-2} d^{-1} at the inner estuary. Additionally, while much of the CO_2 absorbed in summer/autumn is released to the atmosphere in the inner estuarine zone, the summer/autumn CO_2 uptake in the estuary mouth is 4-fold higher than the winter/spring CO_2 released. Unlike most estuarine systems, the PLE acted as a net CO_2 sink of –2 mmol m^{-2} d^{-1} during the period investigated. The balance between CO_2 uptake and emissions in the PLE was modulated by the combination of wind speed, freshwater discharge, water temperature, and outflow/inflow currents. Furthermore, phytoplankton blooms and strong wind-induced vertical mixing lead to highly variable CO_2 exchanges. The highest estuarine CO_2 concentration by autochthonous production indicates heterotrophy in estuarine waters. Part of this carbon produced in the estuary is exported to the coast, as evidenced by the high CO_2 concentration in the estuary mouth. Therefore, the lower estuarine zone resists increased CO_2 concentrations and has overcome regional anthropogenic emissions. The regional FCO_2 range and complex PLE biogeochemistry dynamics need ongoing investigation to improve knowledge of regional CO_2 exchanges and elucidate the role of large estuaries and coastal bays in the global carbon budget.

Keywords: estuaries; carbon dioxide; CO_2 partial pressure; CO_2 fluxes

1. Introduction

Estuaries are known to be large sources of carbon dioxide (CO_2) to the atmosphere (e.g., Cai 2011; Bauer et al. 2013; Evans et al. 2013; Dinauer and Mucci 2017; Yao and Hu 2017; Yao et al., 2020), with the surface water partial pressure of CO_2 (pCO_2) ranging from 350 to 10,000 µatm and the water-air CO_2 net flux (FCO_2) ranging from –5 to 80 mol C m^{-2} $year^{-1}$ (Cai, 2011). This CO_2 outgassing behavior is attributed to intense carbon fixation and respiration in estuarine waters, owing to the higher primary production and leading to high rates of organic matter decomposition. The high amounts and fast cycling of autochthone and allochthone inputs of organic matter are degraded by microbial action, which causes supersaturation of CO_2 in estuarine surface waters (Sunda and Cai 2012). The carbon inputs and their reactions support prominent heterotrophy and contribute to the widespread supersaturation of CO_2, decreasing pH (e.g., Feely et al., 2010; Borges and Abril 2011; Cloern et al. 2014). The changes in estuarine pCO_2 regulate the water-air CO_2 gradients that determine the direction of CO_2 exchanges (Sarma et al. 2001). In addition, estuaries are commonly neglected in global FCO_2 inventories, and estuarine processes are not factored into the global carbon budget (e.g., Cotovicz et al. 2020). Furthermore, estuaries are highly productive regions where natural biogeochemical reaction rates are elevated; thus, understanding CO_2 dynamics in these environments is essential (Sarma et al., 2001).

Patos Lagoon (Figure 1) is the largest choked lagoon in the world (Kjerfve, 1986), and it is connected to the sea by a narrow channel (Castelão and Möller 2003; Marques and Möller 2008; Marques et al. 2009) in extreme southern Brazil (~32°S). The hydrodynamics of the Patos Lagoon Estuary (PLE) are dominated by wind at time scales associated with the passage of frontal systems and the strength of freshwater discharge in the microtidal region (Möller et al. 2001). The seawater intrusions are greater during the autumn due to the more frequent passage of frontal systems. In this case, southerly winds combined with low freshwater input allow flooding and salinization of the water. Northeastern winds occur at the end of winter and during spring, with periods of high freshwater discharge that favor ebb flow. The north and south quadrant winds form vertical salinity structures that can range from a salt wedge to a well-mixed gradient (Möller et al. 2001; Möller and Fernandes 2010). The complex balance between freshwater outflow and oceanic inflow leads to large variations in salinity, which significantly affects physical (e.g., Möller et al. 2001), chemical (e.g., Niencheski et al. 2006; Albuquerque et al. under review) and biological properties (e.g., Haraguchi et al.

2015). Although the PLE is a well-studied environment in terms of estuarine hydrodynamics (e.g., Möller et al. 2001; Möller and Fernandes 2010), biology and physiology of dominant estuarine species, and ecosystem ecology (e.g., Haraguchi et al. 2015; Abreu and Odebrecht 2016; Mendes et al. 2016; Islabão et al. 2017; Odebrecht et al. 2017), very little is known about estuarine carbon biogeochemistry (Albuquerque et al. under review). Recently, the first assessment of the estuarine carbonate system in the region indicated that the surface waters in the lower zone of the PLE have natural alkaline conditions, with an average pCO_2 of ~380 μatm and a supersaturated calcium carbonate environment with respect to both calcite and aragonite (Albuquerque et al. under review). Additionally, the predominant estuarine processes governing changes in the carbonate system in the region were dilution and concentration of salts due to freshwater input and seawater intrusions, respectively. Notwithstanding its socioeconomic and environmental significance (Odebrecht et al. 2017), only a few studies have assessed the chemical changes in estuarine waters in this complex environment (e.g., Niencheski et al. 2006; Baumgarten and Niencheski 2010; Wallner-Kersanach et al. 2016).

Studies on water-air CO_2 exchanges in estuarine regions are mostly located along the European, Asian, Indian, and eastern North American coasts (e.g., Bauer et al. 2013; Evans et al. 2013), while knowledge of CO_2 coastal dynamics in the Southern Hemisphere remains limited. Few studies have addressed the water-air CO_2 exchange systems that border the Brazilian coast (e.g., Noriega et al. 2013; Noriega and Araujo 2014; Cotovicz et al. 2015; Cotovicz et al. 2020; Abril et al. 2021), where highly diversified environments in terms of CO_2 saturation with the atmosphere were found. As a larger body of water in the Southern Hemisphere, a better understanding of the regional behavior of the CO_2 fluxes in the PLE is mandatory for its inclusion in a global CO_2 analysis. Therefore, in this study, we present the first overview of the behavior of the water-air CO_2 exchanges in the lower estuarine zone of the Patos Lagoon (Figure 1) by investigating the pCO_2 drivers, sources of CO_2 in the region, and the temporal variability in the water-air CO_2 fluxes in this environment. This assessment of the intrinsic variability in the CO_2 system in the PLE represents the first step toward understanding both anthropogenic and climatic impacts that may affect the carbon dynamics in the region.

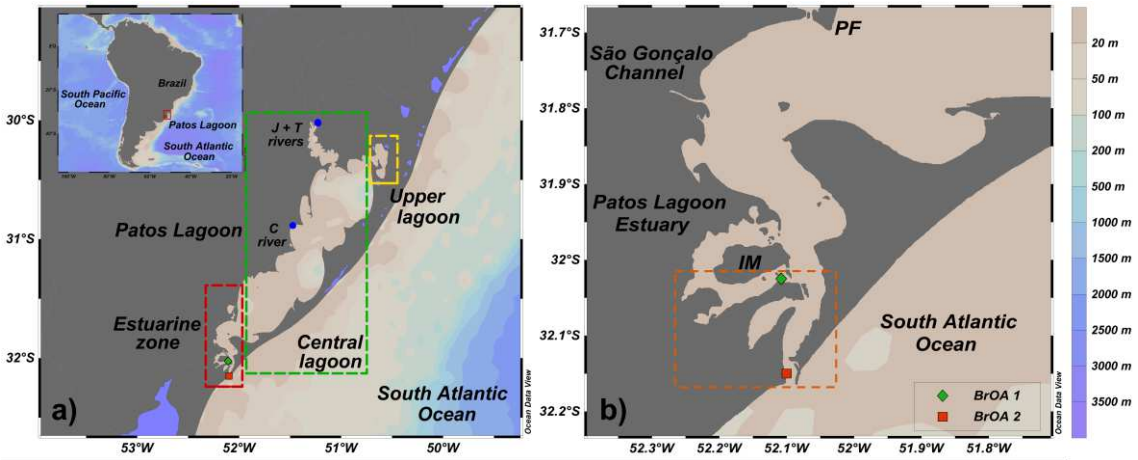

Figure 1: Map of the study region: Patos Lagoon. **(a)** Location of Patos Lagoon and geomorphological divisions for the estuarine zone (red rectangle), central lagoon (green rectangle) and upper lagoon (yellow rectangle). The inset in (a) shows a South American map with the location of Patos Lagoon (red rectangle). Blue dots indicate the regions of freshwater discharge from the Jacuí and Taquari (J + T) and Camaquã (C) Rivers. **(b)** Location of the pier-fixed monitoring BrOA #1 (green diamond) and #2 (red square) stations in the Patos Lagoon Estuary with the southern region highlighted (orange rectangle). Marinheiros Island (IM) and Ponta da Feitoria (PF) are indicated.

2. Data and Methods

2.1 Database from the Brazilian monitoring programs

The databases of the Brazilian Long-Term Ecological Research (BR-LTER; Odebrecht and Abreu 2019; Lemos et al. 2021; dataset available at https://doi.org/10.15468/xmlvxm) and the Brazilian Ocean Acidification Network (BrOA Network; Kerr et al. 2016; dataset available by request at https://carbonteam.furg.br/2-uncategorised/47-monitoramento) were compiled for the study of a four-year monthly time series (May 2017-June 2021) in two zones of the PLE. The pier-fixed station BrOA #1 is in the inner mesomixohaline region, while BrOA #2 is in a more exposed area of the lower euhaline region. The stations are marked by differences in water salinity and hydrodynamics. The physical, biological, and chemical parameters were sampled by BR-LTER and included surface water (~1 m) temperature, salinity, chlorophyll-a (Chl-*a*) and dissolved nutrients (i.e., nitrate, nitrite, silicic acid, and phosphate). The surface water (~1 m) total alkalinity (A_T), total dissolved inorganic carbon (C_T) and pH were sampled by the BrOA Network monitoring program. For more details about the datasets and sampling methodology, the reader is referred to Albuquerque et al. (under review) and Lemos et al. (2021).

2.2 Sampling and determination of physical, chemical, and biogeochemical properties

Surface water temperature and salinity were measured *in situ* by a digital thermometer (± 1°C) and portable refractometer (± 1), respectively. The water sample was collected, and the salinity was further verified in the laboratory by a conductivity meter. Water for A_T analysis was sampled in 500 mL borosilicate glass bottles and fixed with 100 µL of a supersaturated mercury chloride solution to prevent biological activity, following the procedure described by Dickson et al. (2007). The samples were refrigerated to prevent evaporation, and A_T was measured by potentiometric titration in a closed cell (Dickson et al. 2007) with an automated titrator (Metrohm® Titrando 808) and a combined glass-reference electrode (Metrohm® 6.0262.100) at a controlled temperature of 25 ± 0.1°C sustained by a thermostatic bath (Tamson® TLC 15). The analytical precision of the A_T analyses was ± 4.0 µmol kg^{-1} (ranging from $2.3 < A_T < 5.0$ µmol kg^{-1} considering the analyzed sample batches). Water for pH analysis was sampled in 125 mL borosilicate amber flasks, and the pH was potentiometrically determined before two hours after sampling. We used a Metrohm® 913 or 914 pH meter coupled with a glass-reference electrode cell and a temperature sensor. The uncertainty for pH was ≤ 0.05 pH NBS units. The total scale was chosen and further used for pH at *in situ* temperature.

The pCO_2 and other CO_2-carbonate variables not directly measured were estimated through the software CO_2Sys v.2.1 developed by Lewis et al. (1998) and modified by Pierrot et al. (2006). Surface water temperature, salinity, A_T, pH, silicic acid, and phosphate concentrations were used as input parameters. Since the study was performed in an estuarine environment with a broad salinity range, we applied the following set of constants: the K_1 and K_2 dissociation constants of Millero et al. (2006), such as those used in PLE (Albuquerque et al. under review) and other estuary and coastal environments (Liu et al. 2017, Carstensen et al. 2018, Chen et al. 2020); and the sulfate and borate constants of Dickson (1990) and Uppström (1974), respectively. The pCO_2 uncertainty was determined to be ±46 µatm according to Orr et al. (2018). A more detailed description of the sampling procedure and laboratory analysis of A_T and pH and reconstruction of pCO_2 is fully described in Albuquerque et al. (under review).

2.3 Drivers of changes in the estuarine water partial pressure of CO_2

The pCO_2 drivers were calculated based on the seasonal differences in parameters and their corresponding partial derivatives. The differences in pCO_2 were separated into contributions representing the roles of differences in temperature (Temp), salinity (Sal), A_T, and C_T. The relative contributions of the drivers changing pCO_2 (i.e., ΔpCO_2^{drv}) were assessed by converting their relative changes into pCO_2 units (µatm) following Lenton et al. (2012) and Equation 1:

$$\Delta pCO_2^{drv} = \frac{\partial pCO_2}{\partial Temp}\,\Delta Temp + \frac{\partial pCO_2}{\partial Sal}\,\Delta Sal + \frac{\partial pCO_2}{\partial A_T}\,\Delta A_T + \frac{\partial pCO_2}{\partial C_T}\,\Delta C_T, \quad \text{Eq. 1}$$

where ΔTemp, ΔSal, ΔA_T and ΔC_T are the respective differences in the water surface property averages between each season and the previous season in the lower zone of the PLE, considering the sampling period from May 2017 to June 2021. The partial derivatives (δ) were calculated using Equations 2, 3 and 4 (see details in Sarmiento and Gruber 2006), and the term involving temperature was calculated using Equation 5 (Takahashi et al. 2014):

$$\frac{\partial pCO_2}{\partial C_T} = \frac{pCO_2}{C_T}\; x\; Revelle\; Factor, \quad \text{Eq. 2}$$

$$\frac{\partial pCO_2}{\partial A_T} = \frac{pCO_2}{A_T}\; x\; Alkalinity\; Factor, \quad \text{Eq. 3}$$

$$\frac{\partial pCO_2}{\partial Sal} \approx 0.026\; x\; pCO_2, \quad \text{Eq. 4}$$

$$\frac{\partial pCO_2}{\partial Temp}\Delta Temp \approx\; 2pCO_2\; x\; \left[Exp\; \left(0.0423\; x\; \frac{\Delta Temp}{2}\right) - 1\right]. \quad \text{Eq. 5}$$

where the Revelle and Alkalinity factors are 14.2 and –26.5, respectively.

2.4 Water-air CO_2 net flux

The water-air CO_2 fluxes (FCO_2) were obtained by Equation 6:

$$FCO_2 = K_t\, K_s\, \Delta pCO_2, \quad \text{Eq. 6}$$

where K_t is the coefficient for CO_2 transfer velocity as a function of wind speed (U), K_s is the solubility coefficient of CO_2 calculated as a function of both temperature and salinity (Weiss 1974), and ΔpCO_2 is the difference between surface water pCO_2 and atmospheric pCO_2 (pCO_2^{air}). CO_2 is taken up by estuarine water when the FCO_2 value is negative (ingassing), while it is released to the atmosphere when the FCO_2 value is positive (outgassing).

The pCO_2^{air} was calculated following Equation 7:

$$pCO_2^{air} = xCO_2^{air}(pAir - \left(\frac{1.5}{101.325}\right) - pH_2O), \quad \text{Eq. 7}$$

where xCO_2^{air} (ppm) is the mole fraction of atmospheric CO_2 in dry air, obtained from the Mauna Loa Observatory (NOAA ESRL Global Monitoring Laboratory, 2019; Thoning et al. 2021), with data 6 months before the corresponding period due to the atmospheric response between the Northern and Southern Hemispheres (Millero, 2013). pAir is the barometric pressure from the Rio Grande city (Brazil) meteorologic station, and pH_2O (atm) is the water vapor pressure calculated using salinity and temperature (Weiss and Price, 1980).

The main challenge in calculating FCO_2 in estuarine waters is the determination of K_t due to its complex hydrodynamics and varied geomorphology (e.g., Dinauer and Mucci, 2017; Yao et al., 2020). Several different predictive relationships between wind speed and gas transfer velocity of CO_2 have been proposed based on laboratory and field studies (e.g., Jiang et al. 2008; Raymond and Cole 2001; Takahashi et al. 2009). Here, the gas transfer velocity K_t was parameterized using wind speed and the equation from Jiang et al. (2008), which was derived from Raymond and Cole (2001). The parametrization of Jiang et al. (2008) is mostly used in estuarine environments (e.g., Evans et al. 2013; Van Dam et al. 2018; Yao et al. 2020). The following equation is the K_t equation (Equation 8) of Jiang et al. (2008):

$$K_t = (0.314\,U^2 - 0.436\,U + 3.99)\,x\,(Sc/600)^{-0.5}, \quad \text{Eq. 8}$$

where U is the wind speed at 10 m height and Sc is the Schmidt number of CO_2 at *in situ* temperature (Wanninkhof, 2014). Average monthly wind speed data were available from the 8th Meteorology District of the National Institute of Meteorology (8th DISME/INMET) for Rio Grande do Sul State.

The average standard error of the calculated FCO_2 was ± 0.34 mmol m^{-2} d^{-1}. We recalculated K_t from the equation of Raymond and Cole (2001) to verify the sensitivity of FCO_2 based on the equations used. The average differences between the estimations derived from the original application used (Jiang et al. 2008) and the Raymond and Cole (2001) approach were –45.3 ± 44.8 mmol m^{-2} d^{-1}.

2.5 CO_2 estuarine concentration estimates

We followed the approach described in Jiang et al. (2008) to determine the C_T change caused by river–ocean mixing, using C_{Tmr} (Equation 9) to estimate the riverine water input and C_{Tmix} (Equation 10) to estimate ocean mixing at each pier-fixed station (*i*):

$$C_{T_{mr}} = \left(\frac{S_i}{S_{oc}}\right) \times C_{T_{oc}} + \left(\frac{1 - S_i}{S_{oc}}\right) \times C_{T_r}, \quad \text{Eq. 9}$$

$$C_{T_{mix}} = \frac{(S_{oc} - S_i) \times C_{T_r} + (S_i - S_r) \times C_{T_{oc}}}{S_{oc} - S_r}, \quad \text{Eq. 10}$$

where C_{Tr}, S_r, C_{Toc} and S_{oc} are the C_T and salinity river and ocean end-members, respectively, and S_i is the salinity at station *i*.

As there was no continuous sampling during the study period at the mouth of the river or at a fixed point in the ocean, the average values of C_{Tr}, S_r, C_{Toc} and S_{oc} representing the river and ocean most pure conditions were determined from the station closest to the river outlet (BrOA #1; salinity < 5) and from the nearest ocean station (BrOA #2; salinity < 32), respectively. Thus, the C_T and salinity river and ocean end-members were S_r = 2.57, C_{Tr} = 703.37 μmol kg^{-1}, S_{oc} = 31.36, and C_{Toc} = 1648.38 μmol kg^{-1}.

When there is no river influence, the C_T at station *i* can be calculated as follows:

$$C_{T_{m0}} = \frac{S_i}{S_{oc}} \times C_{T_{oc}}, \quad \text{Eq.}$$

where C_{Tmo} is C_T due to water mixing; C_{Toc} and S_{oc} are C_T and salinity at the ocean end-member, respectively; and S_i is the salinity at station *i*.

Then, produced/consumed C_T due to estuarine-biogeochemical processes (C_T^{est}) can be calculated as follows:

$$C_T^{est} = C_{T_i} - C_{T_m}, \quad \text{Eq. 12}$$

where C_{Ti} is C_T at station *i* and C_{Tm} is C_T due the mixing of river and ocean and can be calculated from Equations 9-11. Following the same approach, A_{Tm} and A_T^{est} can be estimated by simply replacing C_T with A_T. For A_T end-members, averages were also defined. A_{Tr} and A_{Toc} were 699.47 and 2087.04 μmol kg^{-1}, respectively.

Finally, the CO_2 estuarine concentration was calculated through the software CO_2Sys v.2.1 (Lewis et al. 1998; Pierrot et al. 2006) using C_T, A_T, salinity, and temperature as input parameters. We used $[CO_2]_{ocean}$, $[CO_2]_{river}$, and $[CO_2]_{est}$ to represent ocean-borne $[CO_2]$, river-borne $[CO_2]$, and estuarine-produced $[CO_2]$, respectively. Aqueous CO_2 ($[CO_2]$) does not mix conservatively, so $[CO_2]_{ocean}$ is the aqueous CO_2 concentration of

the ocean end-member if these were diluted by freshwater with zero C_T, calculated by C_{Tmo} and A_{Tmo} (Equation 12). $[CO_2]_{river}$ is the difference between $[CO_2]$ due to mixing and $[CO_2]_{ocean}$ (Jiang et al. 2008).

$$[CO_2]_{river} = [CO_2]_m - [CO_2]_{ocean}, \quad \text{Eq. 13}$$

$$[CO_2]_{est} = [CO_2]_i - [CO_2]_m, \quad \text{Eq. 14}$$

where $[CO_2]_m$ is $[CO_2]$ if conservative mixing occurred between river and ocean end-members, calculated using C_{Tmr} or C_{Tmix} and A_{Tmr} or A_{Tmix}; $[CO_2]_{ocean}$ is the aqueous CO_2 concentration of the ocean; and $[CO_2]_i$ is the aqueous CO_2 concentration at station *i*. The $[CO_2]$ is consumed when the $[CO_2]$ value is negative, while the $[CO_2]$ is produced in the estuary once the $[CO_2]$ value is positive. When $[CO_2]$ is calculated from C_T and A_T, the annual average temperature of 21.03°C was used since the dissolved $[CO_2]$ is subject to changes in water temperature.

3. Results

3.1 Drivers of seasonal changes in the partial pressure of CO_2

A_T and C_T had the dominant effect on changes in pCO_2, while salinity and temperature had a minor influence on surface pCO_2 (Figure 2). In summer, there was a considerable decrease in pCO_2, driven mainly by an increase in A_T. In autumn, winter and spring, there was an increase in pCO_2; however, its driver was different in each season. The increase in pCO_2 was partially counteracted by the temperature drawdown in autumn. In winter and spring, C_T and A_T had opposite effects on pCO_2 compared with summer and autumn. In winter, the decrease in A_T led to an increase in pCO_2. On the other hand, although C_T decreased considerably, pCO_2 increased in spring.

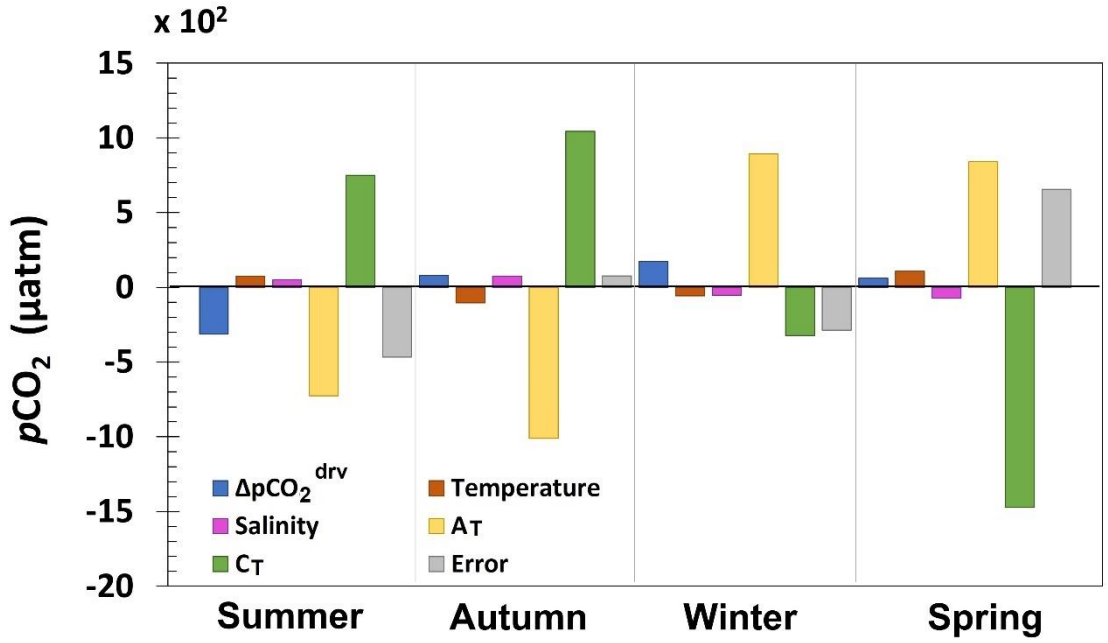

Figure 2: Effects of surface water temperature, salinity, total alkalinity (A_T) and total dissolved inorganic carbon (C_T) on the partial pressure of CO_2 (pCO_2) for each season for the stations located in the lower zone of the Patos Lagoon Estuary region. The variation in each parameter is calculated as the difference between the values of each parameter and their respective averages in previous seasons. The unit of all drivers is the same as that for pCO_2 (µatm), and their magnitudes represent their influence on pCO_2^{sw} changes. The error bars (gray) show the difference between the sum of all drivers and the actual variation in pCO_2 (ΔpCO_2^{drv}), indicating the extent to which the decomposition of pCO_2 into its drivers differs from ΔpCO_2^{drv}. More details are given in the methods section.

3.2 Seasonal and interannual variability in air-water CO_2 net flux

The seasonal cycle of water-air CO_2 net fluxes showed a similar variability pattern in the areas investigated but with different amplitudes at stations BrOA #1 and #2 (Figure 3a and b). At the inner inlet station (BrOA #1), the seasonal amplitude of CO_2 exchanges varied from –38 to 54 mmol m^{-2} d^{-1} and was higher than that found at the mouth of the estuary (BrOA #2), which ranged from –29 to 21 mmol m^{-2} d^{-1}. In addition, although the net CO_2 ingassing during summer/autumn seasons are very close to each other in both areas (average of ~ –16 ± 23 and ~ –18 ± 28 mmol m^{-2} d^{-1}), the same is not true for the behavior of the CO_2 exchange during winter/spring seasons. The winter/spring net CO_2 outgassing is 10-fold higher in the inner inlet zone (average of 22 ± 40 mmol m^{-2} d^{-1}) than that found near the more sea-exposed zone (average of 2 ± 31 mmol m^{-2} d^{-1}). In general, the net CO_2 outgassing was highest in spring (October and November) at the BrOA #1 station, although this behavior was also observed during winter. The lower estuarine zone of the Patos Lagoon acts as net CO_2 ingassing during half the year, from

December to May, while a behavior of water-air CO_2 quasi-equilibrium is observed from June to September in the mouth of the estuary (Figure 3a and b).

Despite the high monthly variability and the marked seasonal cycle of the CO_2 exchanges observed in the PLE (Figures 3 and 4), during the 4-year period analyzed, the inner inlet zone behaved as net CO_2 outgassing to the atmosphere (2.9 ± 41.4 mmol m^{-2} d^{-1}), in contrast to the behavior as an estuarine net CO_2 sink zone (-7.2 ± 33.3 mmol m^{-2} d^{-1}) observed in the area close to the ocean. Thus, the net behavior during the entire period revealed that the lower zone of the PLE behaved as an area of CO_2 uptake (-2.1 ± 27.2 mmol m^{-2} d^{-1}; Figure 4).

In 2019, there was intense CO_2 uptake (-23.9 ± 33.8 mmol m^{-2} d^{-1}) by the PLE surface waters, while in 2018, the region often released CO_2 (7.5 ± 41.3 mmol m^{-2} d^{-1}) to the atmosphere. The CO_2 outgassing was high in 2017. However, we did not evaluate the summer data when most of the CO_2 was absorbed. For 2021, we did not consider the winter/spring season, when CO_2 emissions are higher (Figure 4). According to our analysis, the water-air net CO_2 fluxes evolve at periods of 3 and 6 months and one year, mainly at the BrOA #1 station (Figure S1).

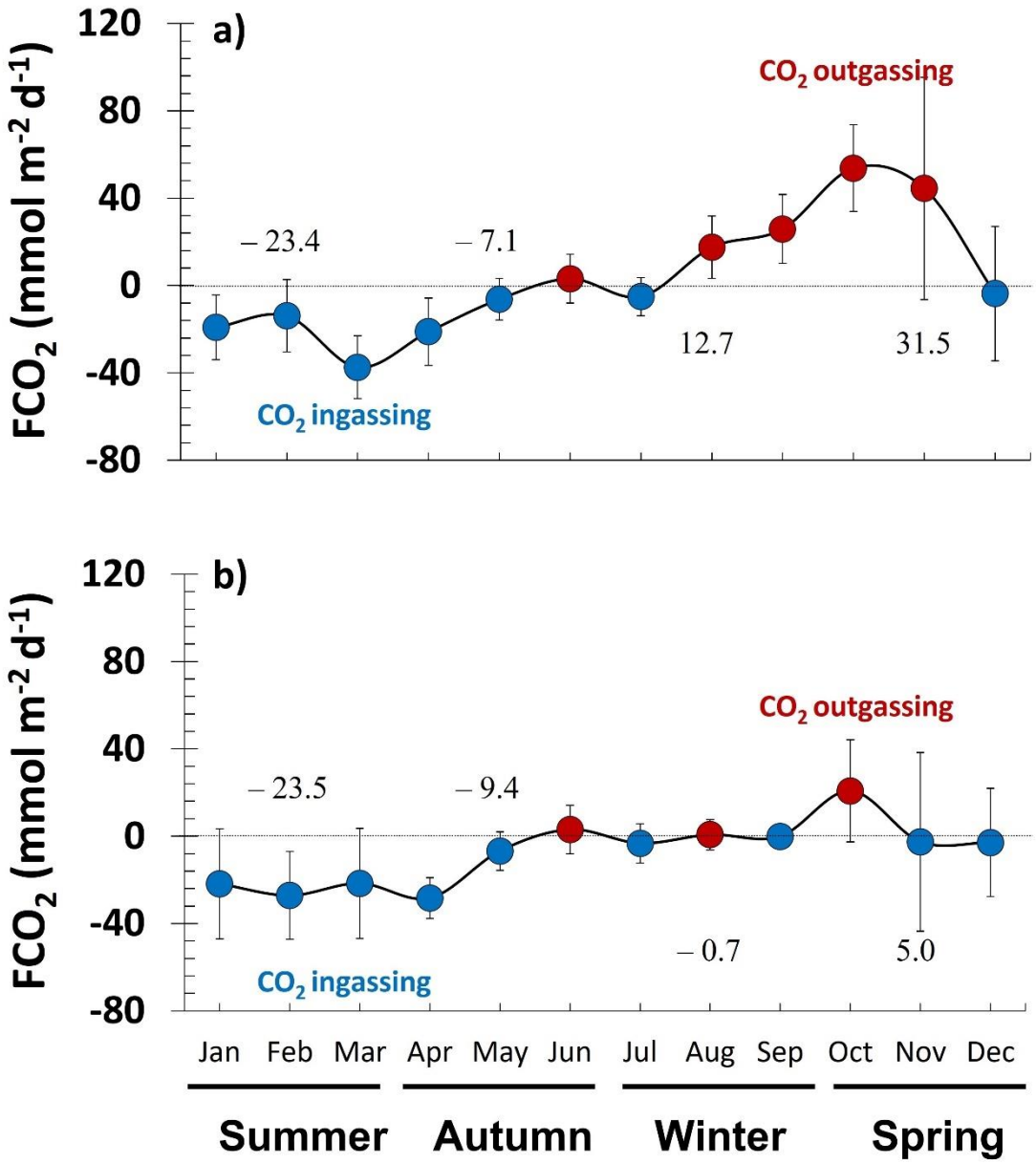

387

388 **Figure 3:** Seasonal cycle of surface water-air CO_2 net flux (FCO_2) of the lower zone of the Patos Lagoon
389 Estuary obtained from May 2017 to June 2021 at the **(a)** pier-fixed station BrOA #1 (inner inlet) and **(b)**
390 BrOA #2 (sea-exposed area). The error bars indicate the standard error of each month. The values indicate
391 the average FCO_2 for each season. Blue dots indicate months of CO_2 ingassing, while red dots indicate
392 months of CO_2 outgassing.

393

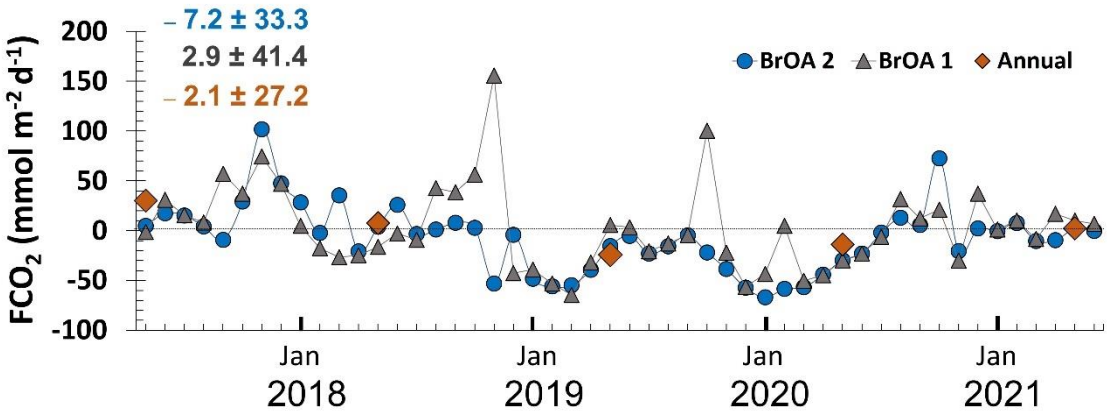

Figure 4: Monthly and interannual variability in water-air surface CO_2 net flux (FCO_2) for the BrOA #1 (gray triangles) and BrOA #2 (blue dots) stations at the Patos Lagoon Estuary from May 2017 to June 2021. The orange diamonds depict the annual averages (note that 2017 and 2021 do not consider all the seasons). The FCO_2 annual average and standard deviation for each estuarine station (color indicated by the legend) and joined regions (orange) are indicated in the top left.

3.3 River-borne, ocean-borne, and estuarine-generated CO_2

The seasonality of CO_2 concentrations is relatively different in each region analyzed. At the inner inlet station, the seasonal cycle of the CO_2 estuarine is marked and varies from –17 to 39 µmol kg^{-1}, while at the mouth of the estuary, the CO_2 estuarine varies from –9 to 31 µmol kg^{-1} (Figure 5a and b). Despite the difference in estuarine, ocean and river CO_2 concentrations, the same variation was observed at both the inner inlet and estuarine mouth stations. The CO_2 concentrations averaged 1.8 ± 0.4 µmol kg^{-1} for the ocean, 2.2 ± 0.5 µmol kg^{-1} for the river and 5.2 ± 3.2 µmol kg^{-1} for all lower zones of the estuary during the summer/autumn seasons, while in the winter/spring seasons, the CO_2 estuarine concentration was more than 2-fold higher (average of ~ 13 ± 4.5 µmol kg^{-11}) than that in other seasons. Thus, the lower estuarine zone of the Patos Lagoon acts as a region of production of estuarine CO_2, mainly during months of high freshwater discharge into the lagoon (i.e., end of winter and spring; Figures 5 and S2), with great magnitudes of CO_2 in the more protected embayment and less hydrodynamic zones. Regarding river-borne CO_2, the behavior of the PLE was different from that observed for estuarine CO_2. The river-borne CO_2 was higher in periods of high freshwater discharge, while in months where the freshwater discharge was low, the input of CO_2 with marine sources was intense.

Despite the small difference, the inner inlet zone produced more CO_2 (11.8 ± 12.6 µmol kg^{-1}) than the exposed area (9.1 ± 10.0 µmol kg^{-1}). At the end of 2018, there was a

decrease in CO_2 estuarine production and an increase in CO_2 estuarine consumption in the region, with more CO_2 estuarine consumption at the mouth of the estuary (Figure 5b) than in the sheltered area. From July 2019, the ocean-borne CO_2 increased at both stations.

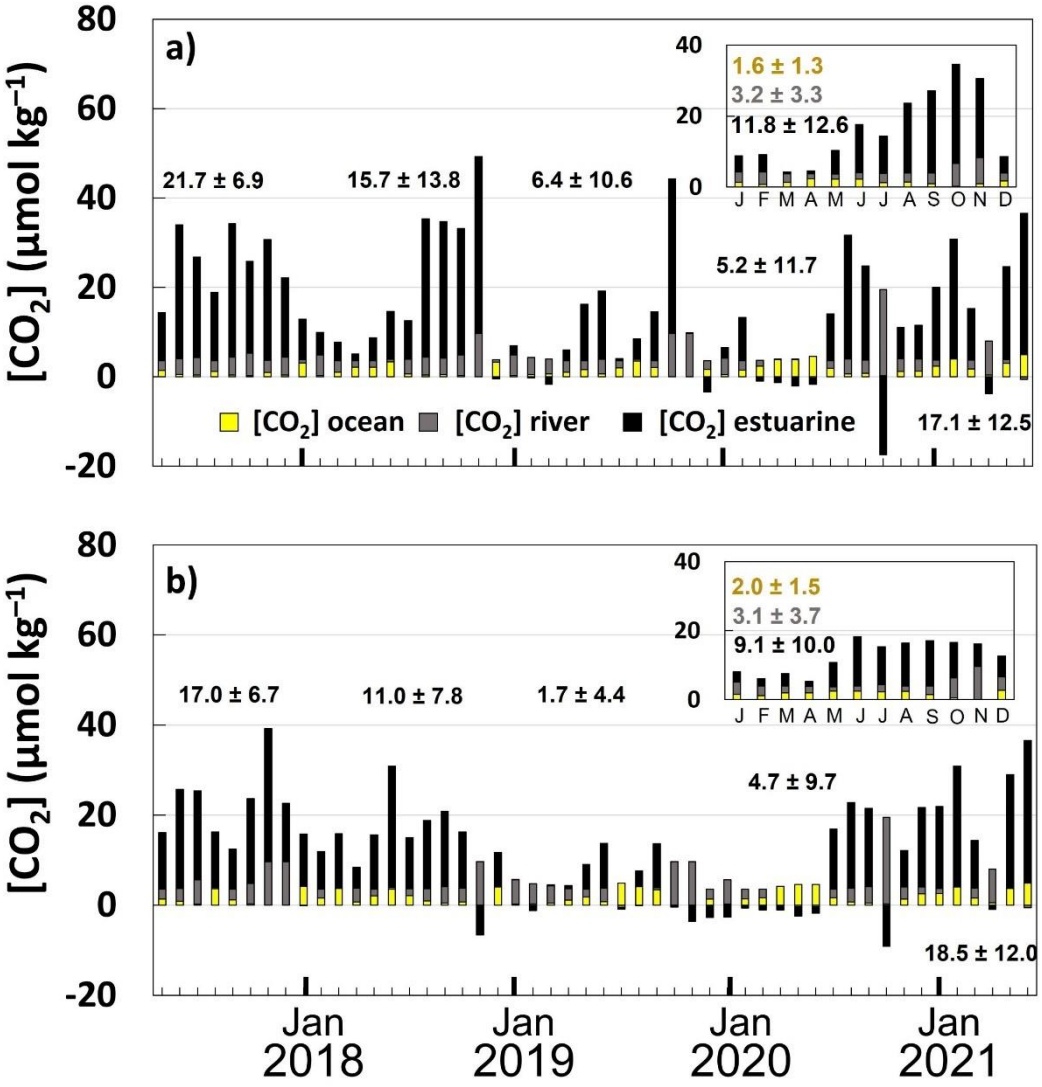

Figure 5: Monthly variability in aqueous surface CO_2 concentration ($[CO_2]_{ocean}$; yellow bars, $[CO_2]_{river}$; gray bars, and $[CO_2]_{estuarine}$; black bars) for the stations located in the lower zone of the Patos Lagoon Estuary from May 2017 to June 2021 in the **(a)** BrOA #1 and **(b)** BrOA #2 pier-fixed stations with annual average and standard deviation for CO_2 estuarine concentration. The seasonal cycle is inserted in the top right with the average and standard deviation for each CO_2 concentration.

4. Discussion

4.1 Seasonal drivers of pCO_2

The A_T and C_T variations were the main causes of changes in pCO_2 variability. The concentration of salts and dilution are the main processes identified in the pCO_2 variation, indicated by increases (summer/autumn) and decreases (winter/spring) in A_T and C_T (Figure 2). The lower estuarine zone of the Patos Lagoon shows a high amplitude of A_T (479 to 2,245 μmol kg^{-1}) and C_T (500 to 2,040 μmol kg^{-1}; Albuquerque et al. under review), related to periods of increased (winter/spring) freshwater discharge and seawater inflows (summer/autumn). Furthermore, the PLE is a region with high organic matter concentrations due to large continental inputs, abundant macrophyte communities and local anthropogenic sources (Baumgarten and Niencheski 2010) that lead to heterotrophy and macroalgal blooms in spring, which directly influence the carbon concentration (Haraguchi et al. 2015; Lanari and Copertino 2017; Lanari et al. 2018). Another factor is the hydrodynamic processes that lead to large variations in salinity (Haraguchi et al. 2015). These features aid in the final behavior of A_T, C_T and salinity and indirectly affect the pCO_2 variation.

The estimated deviations of the analysis (Figure 2) are an indication that some estuarine processes were not yet accounted for in the pCO_2 changes, such as the influence of phytoplankton biomass (e.g., Lee et al. 2006; Cai 2011) and the property changes related to groundwater input (e.g., Sadat-Noori et al. 2016; Jeffrey et al. 2018), which configures a current limitation and a challenge for further studies. The higher freshwater discharge in late winter and during spring brings a higher concentration of organic matter, supporting phytoplankton blooms in the PLE (Albuquerque et al. under review). The deviations observed in summer and spring are probably due to photosynthesis rates (Albuquerque et al. under review), which leads to a decrease in pCO_2 levels. Groundwater may be enriched in dissolved carbon species; therefore, groundwater input affects the carbon concentration in water (Sadat-Noori et al. 2016), increasing the pCO_2 concentration. Although the approach used in this study is mostly used to infer the main variables and processes affecting the pCO_2 distribution for oceanic waters (e.g., Takahashi et al. 2014; Moreau et al. 2017; Monteiro et al. 2020), it is also a useful approach in estuarine systems that have periods of waters with high salinity signals. However, as previously indicated, further investigation of coupled estuarine-biogeochemical processes must be performed to reduce uncertainties, mainly during freshwater dominance periods in the estuarine system.

4.2 Water-air CO_2 fluxes and CO_2 concentrations

488 Estuarine systems are significant sources of CO_2 to the atmosphere with recognized
489 relevance for regional and global carbon budgets (e.g., Guo et al. 2009; Gupta et al. 2009;
490 Jeffrey et al. 2018; Joesoef et al. 2015), and estuarine lower zones realize approximately
491 23 mmol m^{-2} d^{-1} (Chen et al. 2013). The magnitude of the CO_2 exchanges in the lower
492 estuarine zone of the PLE is variable, with values ranging from –66 to 155 mmol m^{-2} d^{-1}
493 and a net CO_2 ingassing average of –2 mmol m^{-2} d^{-1} for the 4-year period investigated
494 here (Figure 4; Table 1). The variations observed in the lower zone of the PLE display a
495 typical distribution pattern seen in other estuarine environments (Table 1), mainly in
496 shallow estuaries dominated by freshwater discharge, such as the PLE (e.g., Evans et al.
497 2013; Koné et al. 2009; Table 1). Moreover, the same range of water-air CO_2 exchanges
498 observed in the subtropical PLE can be found in other tropical estuarine environments in
499 Brazil (e.g., Cotovicz et al. 2020; Noriega and Araujo 2014), shifting between periods of
500 CO_2 ingassing and CO_2 outgassing to the atmosphere over the year.

Table 1: Comparison between the range of water-air CO_2 flux (FCO_2) from previous estuarine studies around the world and the current study. The studies are organized first by country and second by climate.

Reference	Estuary location	Country	Climate	Type	Period	Water-air FCO_2 (range in mmol m^{-2} d^{-1})
This study	Lower zone of PLE South Brazil	Brazil	Subtropical	Freshwater discharge dominated	May 2017 to June 2021	−66 to 155
Cotovicz et al. 2020	Paraíba do Sul River Southwestern Brazil	Brazil	Tropical	Freshwater discharge dominated	February 2017 October 2017 March 2018	−37.8 to 216.1
Noriega and Araujo 2014	North and Northeast Brazilian estuaries	Brazil	Tropical and semiarid	Various	July 2012 to June 2013	2.4 to 175.2
Chen et al. 2020	Chesapeake Bay	USA	Subtropical	Partially mixed and microtidal	March to December 2016 February 2019	−11.2 to 92.4
Yao and Hu 2017	Mission-Aransas	USA	Subtropical semiarid	Freshwater discharge dominated	May 2014 to April 2015	−13.5 to 380.3
Ho et al. 2014	Shark River	USA	Tropical	Mangrove	November 2010 November 2011	20 to 118
Evans et al. 2013	Columbia River	USA	Temperate	Freshwater discharge dominated	August 2007 November 2007 April 2008 June 2008 September 2008	−53.0 to 193.2
Joesoef et al. 2015	Delaware	USA	Temperate	Freshwater discharge dominated	June 2013 August 2013 October 2013 November 2013 March 2014 July 2014 August to September 2014 October to November 2014 December 2014	−21.0 to 129.1

Crosswell et al. 2012	Neuse River	USA	Temperate	Macrotidal	June 2009 to July2010	−38 to 271
Dinauer and Mucci 2017	St. Lawrence	Canada	Temperate	Freshwater discharge dominated	July 2003 June 2006 May 2007 July 2007 June 2009 July 2009 July 2010 May 2011 June 2013 May 2016	−21.9 to 28.4
Koné et al. 2009	Lagoon's system	Ivory Coast	Tropical	Microtidal	June to July 2006 September 2006 November to December 2006 March 2007	−20.0 to 186.2
Gupta et al. 2009	Cochin	India	Tropical	Microtidal	February 2005 April 2005 September 2005	64 to 274
Guo et al. 2009	Pearl River	China	Subtropical	Freshwater discharge dominated	November 2002 February 2004 January 2005 August 2005 April 2007	−25.8 to 907.7
Oliveira et al. 2017	Tagus	Portugal	Temperate	Tide dominated	1999 to 2007	16.6 to 347.1
Borges et al. 2004	Scheldt	Netherlands	Temperate	Macrotidal	November 2002 April 2003	31 to 2,189
Bozec et al. 2012	Loire	France	Temperate	Tide dominated	April 2009 July 2009 October 2009 February to March 2010	−9 to 140
Flecha et al. 2015	Guadalquivir	Spain	Mediterranean	Mesotidal	November 2007 to August 2009	−0.7 to 83.9

Maher and Eyre 2012	Hastings River	Australia	Temperate	Wave dominated	June 2006	−8.7 to 25.3
	Camden Haven	Australia	Temperate	Wave dominated	October 2006	−16.5 to 12
	Wallis Lake	Australia	Temperate	Wave dominated	February 2007 April 2007	−30.4 to 26.2

503

Significant seasonal variation in the water-air CO_2 fluxes between summer/autumn and winter/spring was observed in the lower zone of the PLE. The results presented here demonstrate that the region experienced periods of both CO_2 ingassing (between December and May) and CO_2 outgassing (between June and November), mainly in protected areas along the estuary (Figure 3b). CO_2 exchanges are modulated by winds (Wanninkhof 2014), different hydrodynamic conditions and/or extreme events (Sims et al. 2021). The higher the wind speed is, the greater the influence on the gas exchange between the surface water and the atmosphere; thus, wind speed can play a crucial role in estuarine CO_2 fluxes (e.g., Yao et al. 2020) by exchanging momentum with the atmosphere. In addition, a shallower environment responds faster to wind action (Moller et al. 2001; Lanari and Copertino 2017), which seems to favor fast air-water gas exchange (Yao et al. 2020) and increased CO_2 gradient magnitudes. The water-air CO_2 fluxes in the lower zone of the PLE follow the seasonal pattern of freshwater discharge, which is what occurred with the variability in the carbonate system parameters (Albuquerque et al. under review). In late winter and spring, the freshwater discharge is higher (Marques 2012), and consequently, the entry of organic matter promoting significant heterotrophy in relation to CO_2 is also higher, which is what occurs in the tropical coastal systems in northern and northeastern Brazil (Noriega and Araújo 2014). In the same period, the higher wind speed (~ 4.0 m/s; Figure S2) leads to higher gas transfer velocity in this period with respect to that of summer and autumn. The inner inlet station receives more influence from the freshwater discharge and has a high residence time, leading to an increase in CO_2, while the sea-exposed station is close to the ocean and directly influenced by seawater dynamics and outflow/inflow currents (Möller et al. 2001; Lisboa 2015). Thereafter, CO_2 outgassing in the inner inlet zone should be mainly related to heterotrophic respiration and degradation of organic matter generated on a larger scale by the influence of freshwater discharge, even though this area is also influenced by resuspension of fine bottom sediments (Moller et al. 2001; Lanari and Copertino 2017).

The phytoplanktonic community composition exerts a fundamental role in CO_2 uptake via photosynthesis. In the PLE, diatoms are the dominant phytoplankton group, followed by cyanobacteria, flagellates, dinoflagellates, and chlorophytes along the coastal offshore gradient (Islabão et al. 2017). Microphytoplanktonic diatoms tend to show a higher capacity for capturing CO_2 in water (e.g., Hopkinson et al. 2011) than nano- and picoplanktonic species, which helps to balance the carbon concentration. The production of CO_2 was lower in the more sea-exposed area than in the inner inlet station, suggesting

that the abundance of diatoms in the region closest to the coast is higher due to local hydrodynamics, mainly at the end of winter and spring. Moreover, in spring (October and November), the blooms caused by biological activity combined with vertical mixing due to the higher wind intensity lead to highly variable water-air CO_2 fluxes in the lower zone of the PLE (Figure 3). Despite the different tide regimes, these seasonal conditions are similar to those previously observed in the macrotidal Neuse River estuary (Crosswell et al. 2012) and microtidal Aby Lagoon (Koné et al. 2009). The water temperature influences the CO_2 fluxes because water-air CO_2 exchanges depend on the gas transfer velocity, which is further induced by temperature that changes the solubility of gas in water (Wanninkhof 2014). The higher summer temperatures combined with the CO_2-unsaturated waters from the ocean turn the region into a CO_2 sink in summer and autumn. In general, freshwater input, wind and water temperature are important in the exchange of CO_2; nevertheless, residence time and phytoplanktonic composition also modulate the CO_2 dynamics in different areas of the lower zone of the PLE over the seasons.

The production or consumption of CO_2 is an indicator of estuarine-biogeochemical processes (Yao et al. 2020) and plays a crucial role in determining the water-air CO_2 fluxes of the lower zone of the PLE. Most of the CO_2 released into the atmosphere is produced in the PLE itself. The high freshwater discharge between the end of winter and spring carries organic matter (Niencheski and Windom 1994; Niencheski et al. 2006) that favors photosynthetic respiration and degradation of organic carbon. These processes intensify the production of carbon for the estuary. Although the source is the river, heterotrophy occurs in the estuary because there is more time for the decomposition of organic matter. During this same period, CO_2 inputs from the river are also significant. These two CO_2 sources contribute to CO_2 supersaturation and outgassing to the atmosphere. Therefore, the observed seasonal pattern of CO_2 fluxes and different CO_2 sources suggest that heterotrophy controls the metabolic status of the estuarine waters, mainly in the inner areas of the PLE. In addition, the produced carbon is exported to the coast, which contributes to the high concentration of CO_2 in the mouth of the estuary. This region is a channel with high hydrodynamics (Möller et al. 2001), which allows faster currents and more intense water exchanges. Thus, this area prevents the surface water from CO_2 supersaturation by releasing the gas into the atmosphere.

The interannual variability in estuarine properties and processes in the PLE is influenced by El Niño-Southern Oscillation (ENSO) events (e.g., Odebrecht et al. 2017; Albuquerque et al. under review). The warm phase of ENSO, El Niño, is characterized

by abnormal heating of surface waters in the tropical Pacific Ocean. ENSO affects the regional and global climate, changing the wind patterns worldwide and thus affecting the rainfall patterns in tropical and midlatitude regions (e.g., Cai et al. 2020). Between May 2017 and June 2021, two ENSO events were identified. These events included one El Niño event (in 2017/2018; ENSO warm phase; INPE 2021) and one La Niña event (in 2020/2021; ENSO cold phase; INPE 2021). Under El Niño conditions, freshwater discharge is above the average level (~1770 m^3 s^{-1}), and the opposite is true under La Niña conditions (Vaz et al. 2006; Seeliger and Odebrecht 2010). The decreased water-air CO_2 fluxes from the beginning of monitoring, the increased CO_2 exchanges in the last two years (Figure 4) and the composition of CO_2 (Figure 6) are likely associated with the change from moderate El Niño (2017–2018) to the beginning of La Niña conditions (2019–2020). However, since the time series is relatively short, with some years (2017 and 2021) having missing months, further discussion on this matter is inhibited. Future research focusing on longer time series is still needed to better characterize the role of climate mode teleconnections with changes in the water-air CO_2 exchanges in the PLE.

Finally, it is worth mentioning that at the end of 2018 (October to December) and between November 2019 and January 2020, there was a dredging event in the port access channel located in the estuary (Mirlean et al. 2020). These dredging activities resuspend the sediment, allowing nutrients and carbon to return to the water column and producing some impacts (e.g., water chemical alteration, mud deposition, and changes in the benthos composition), and a monitoring program should always be considered to evaluate their environmental consequences (Torres and Philomena 2013; Mirlean et al. 2020). The environmental impacts associated with the dredging process and spoil disposal can be characterized by direct effects on organisms and habitats and indirect effects attributed to alterations in water quality. Thus, in addition to likely ENSO effects on the region, the behavior of the studied area as a CO_2 ingassing zone (Figure 4) and the increase in estuarine CO_2 consumption from that period (Figure 5) onward may also be influenced by changes in the water properties and water-sediment processes caused by dredging, despite the controversial about the causes and consequences of mud deposition events along the coast (Calliari et al. 2022; Mirlean et al. 2020, 2021; Garcia et al. 2021).

5. Conclusion

Overall, the estuarine ecosystem of the Patos Lagoon behaved as summer/autumn CO_2 ingassing and winter/autumn CO_2 outgassing to the atmosphere. The combined effect of wind speed, continental freshwater discharge, inflow/outflow currents, water temperature, biological activity, and water residence time is responsible for the modulation of the CO_2 exchange in the PLE. However, comparing the different areas of the PLE lower zone, we noticed non-similar forcings acting on the variation in the CO_2 concentration. The water-air CO_2 flux variations at the mouth of the estuary were mainly driven by the balance between the seawater dynamics and freshwater discharge input/output, which influences the scenario of a CO_2 sink. In the inner estuary, heterotrophic respiration and degradation of organic matter contributed to CO_2 outgassing to the atmosphere between the end of winter and spring. Autochthonous production was responsible for the highest concentration of CO_2, indicating heterotrophy in the estuarine surface water. Part of the carbon produced is exported to the coast, contributing to a high concentration of CO_2 in the mouth of the estuary. Therefore, this study shows that the lower zone of the PLE is resilient to high CO_2 concentrations and has been able to overcome anthropogenic emissions in the region. Hence, long-term monitoring programs must continue to improve the understanding of CO_2 exchange variability and help shed light on the role played by the PLE on the global carbon budget.

References

Abreu PC, Marangoni J, Odebrecht C (2016) So close, so far: differences in long-term chlorophyll a variability in three nearby estuarine-coastal stations. Marine Biology Research. https://doi.org/10.1080/17451000.2016.1189081

Abril G, Libardoni BG, Brandini N et al (2021) Thermodynamic uptake of atmospheric CO_2 in the oligotrofic and semiarid São Francisco estuary (NE Brazil). Marine Chemistry. https://doi.org/10.1016/j.marchem.2021.103983

Albuquerque C, Kerr R, Monteiro T et al (Under review) Seasonal and interannual in the carbonate system parameters of the Patos Lagoon Estuary.

Bauer JE, Cai WJ, Raymond PA et al (2013) The Changing Carbon Cycle of the Coastal Ocean. Nature. https://doi.org/10.1038/nature12857

Baumgarten MGZ, Niencheski LFH (2010) A coluna sedimentar como reservatório e fonte de nutrientes em enseadas estuarinas. Tropical Oceanography Online. 38:88–104

Borges AV, Abril G (2011) Carbon Dioxide and Methane Dynamics in Estuaries. Estuarine and Coastal Science. https://doi.org/10.1016/B978-0-12-374711-2.00504-0

Borges AV, Delille B, Schiettecatte L et al (2004) Gas transfer velocities of CO_2 in theree European estuaries (Randers Fjord, Scheldt, and Thames). Limnology and Oceanography. 49:1630–1641

Bozec Y, Cariou T, Macé E et al (2012) Seasonal dynamics of air-sea CO_2 fluxes in the inner and outer Loire estuary 9NW Europe). Estuarine, Coastal and Shelf Science. https://doi.org/10.1016/j.ecss.2011.05.015

Cai W (2011) Estuarine and coastal ocean carbon paradox: CO_2 sinks or sites of terrestrial carbon incineration? Annual Review of Marine Science. https://doi.org/10.1146/annurev-marine-120709-142723

Cai W, McPhaden MJ, Grimm AM et al (2020) Climate impacts of the El Niño-Southern Oscillation on the South America. Nature Reviews Earth & Environment. https://doi.org/10.1038/s43017-020-0040-3

Calliari LJ, Machado AA, Marroig P et al (2020) Mud deposits at Cassino beach: role of dredging. Geo-Marine Letters. https://doi.org/10.1007/s00367-019-00619-6

Carstensen J, Chierici M, Gustafsson BG, Gustafsson, E (2018) Long-term and seasonal trends in estuarine and coastal carbonate systems. Global Biogeochemical Cycles. https://doi.org/10.1002/2017GB005781

Castelão RM, Möller OO (2003) Sobre a circulação tridimensional forçada por ventos na Lagoa dos Patos. Atlântica, 25:91–106

Chen B, Cai W, Brodeur JR et al (2020) Seasonal and spatial variability in surface pCO_2 and air-water CO_2 flux in the Chesapeake Bay. Limnology and Oceanography. https://doi.org/10.1002/lno.11573

Chen C-TA., Huang T-H, Chen, Y-C et al (2013) Air-sea exchanges of CO_2 in the world's coastal seas. Biogeosciences. https://doi.org/10.5194/bg-10-6509-2013

Cloern JE, Foster SQ, Kleekner AE (2014) Phytoplankton primary production in the world's estuarine coastal ecosystems. Biogeosciences. 11:2477–2501

Cotovicz LC, Knoppers BA, Brandini N, et al (2015) A strong CO_2 sink enhanced by eutrophication in a tropical coastal embayment (Guanabara Bay, Rio de Janeiro, Brazil). Biogeosciences. https://doi.org/10.5194/bg-12-6125-2015

Cotovicz LC, Vidal LO, Rezende CE et al (2020) Carbon dioxide sources and sinks in the delta of the Paraíba do Sul River (Southeastern Brazil) modulated by carbonate thermodynamics, gas exchange and ecosystem metabolism during estuarine mixing. Marine Chemistry. https://doi.org/10.1016/j.marchem.2020.103869

Crosswell JR, Wetz MS, Hales B, Paerl HW (2012) Air-water CO_2 fluxes in the microtidal Neuse River estuary, North Carolina. Journal of Geophysical Research. https://doi.org/10.1029/2012JC007925

Dickson AG, Sabine CL, Christian JR (2007) Guide to Best Practices for Ocean CO_2 Measurements. North Pacific Marine Science Organization, Sidney.

676 Dickson AG (1990) Thermodynamics of the dissociation of boric acid in synthetic
677 seawater from 273.15 to 318.15 K. Deep-Sea Res. 37:755–766

678 Dinauer A, Mucci A (2017) Spatial variability in surfasse-water pCO_2 and gas exchange
679 in the world's largest semi-enclosed estuarine system: St. Lawence Estuary (Canada).
680 Biogeoscience. https://doi.org/10.5194/bg-14-3221-2017

681 Evans W, Hales B, Strutton PG (2013) pCO_2 distributions and air-water CO_2 fluxes in the
682 Columbia River estuary. Estuarine, coastal and shelf science. 117:260–272

683 Feely RA, Doney SC, Cooley SR (2010) Ocean acidification: Present conditions and
684 future changes in a high CO_2 world. Oceanography. 22:36–47

685 Flecha S, Huertas IE, Navarro G, et al (2015) Air–Water CO_2 Fluxes in a Highly
686 Heterotrophic Estuary. Estuaries and Coasts. https://doi.org/10.1007/s12237-014-9923-1

687 Garcia CAE, Evangelista H, Möller, OO (2021) Comments on -Dredging in an estuary
688 causes contamination by fluid mud on a tourist ocean beach. Evidence via REE ratios- by
689 N. Mirlean, L. Calliari, and K. Johannesson in Marine Pollution Bulletin 159 (2020)
690 111495. Marine Pollutioon Bulletin. https://doi.org/10.1016/j.marpolbul.2021.112115

691 Gupta GVM, Thottathil SD, Balachandran KK et al (2009) CO_2 supersaturation and net
692 heterotrophy in a tropical estuary (Cochin, India): influence of anthropogenic effect.
693 Ecossystem. https://doi.org/10.1007/s10021-009-9280-2

694 Guo X, Dai M, Zhai W et al (2009) CO_2 flux and seasonal variability in a large subtropical
695 estuarine system, the Pearl River Estuary, China. Journal of Geophysical Research.
696 https://doi.org/10.1029/2008JG000905

697 Haraguchi L, Carstensen J, Abreu PC, Odebrecht C (2015) Long-term changes of the
698 phytoplankton community and biomass in the subtropical shallow Patos Lagoon Estuary.
699 Estuarine, Coastal and Shelf Science. 162:76–87

700 Ho DT, Ferrón S, Engel VC et al (2014) Air-water gas exchange and CO2 flux in a
701 mangrove-dominated estuary, Geophysical Research Letter.
702 https://doi.org/10.1002/2013GL058785

703 Hopkinson BM, Dupont CL, Allen AE, Morel FMM (2011) Efficiency of the CO_2-
704 concentrating mechanism of diatoms. Proceeding of the National Academy of Sciences
705 of the United States of America. https://doi.org/10.1073/pnas.1018062108

706 INPE. 2021. http://enos.cptec.inpe.br/. Accessed on 17 August 2021.

707 Islabão CA, Mendes CRB, Detoni AMS, Odebrecht C (2017) Phytoplankton community
708 structure in relation to hydrographic features along a coast–to–offshore transect on the
709 SW Atlantic continental shelf. Continental shelf research.
710 https://doi.org/10.1016/j.csr.2017.10.003

711 Jeffrey LC, Maher DT, Santos IR et al (2018) The spatial and temporal drivers of pCO_2,
712 pCH_4 and gas transfer velocity within a subtropical estuary. Estuarine, Coastal and Shelf
713 Science. https://doi.org/10.1016/j.ecss.2018.04.022

714 Jiang LQ, Cai W, Wang Y (2008) A comparative study of carbon dioxide degassing in
715 river- and marine dominated estuaries. Limnology and Oceanography.
716 https://doi.org/10.4319/lo.2008.53.6.2603

717 Joesoef A, Huang W-J, Gao Y, Cai, W-J (2015) Air-water fluxes and sources of carbon
718 dioxide in Delaware Estuary: spatial and seasonal variability. Biogeosciences.
719 https://doi.org/10.5194/bg-12-6085-2015

720 Kerr R, Da Cunha LC, Kikuchi RKP et al (2016) The Western South Atlantic Ocean in a
721 high-CO_2 world: current measurement capabilities and perspectives. Environmental
722 Management. https://doi.org/10.1007/s00267-015-0630-x

723 Koné YJM, Abril G, Kouadio KN et al (2009) Seasonal variability of carbon dioxide in
724 the rivers and lagoons of ivory coast (West Africa). Estuaries and Coasts.
725 https://doi.org/10.1007/s12237-008-9121-0.

726 Lanari M, Copertino M (2017) Drift macroalgae in the Patos Lagoon Estuary (southern
727 Brazil): effects of climate, hydrology and wind action on the onset and magnitude of
728 blooms. Marine Biology Research (online).
729 https://doi.org/10.1080/17451000.2016.1225957

730 Lanari M, Copertino M, Cooling LA, Bom FC (2018) The impact of short-term
731 depositions of macroalgal blooms on widgeon-grass meadows in a river-dominated
732 estuary. Harmful algae. https://doi.org/10.1016/j.hal.2018.07.006

733 Lee K, Tong LT, Millero FJ et al (2006) Global relationships of total alkalinity with
734 salinity and temperature in surface waters of the world's oceans. Geophysical Research
735 Letters. https://doi.org/10.1029/2006GL027207

736 Lemos VM, Lanari M, Copertino M et al (2021) Patos Lagoon Estuary and adjacent
737 marine coastal biodiversity long-term data. Earth Syst. Sci. Data Discuss. [preprint].
738 https://doi.org/10.5194/essd-2021-353

739 Lenton A, Metzl N, Takahashi T (2012) The observed evolution of oceanic pCO_2 and its
740 drivers over the last two decades Global Biogeochemical Cycles.
741 https://doi.org/10.1029/2011GB004095

742 Lewis E, Wallace D, Allison LJ (1998) Program developed for CO_2 system calculations.
743 Carbon Dioxide Information Analysis Center, USA.

744 Lisboa PV (2015) Escalas temporais de transporte do estuário da Lagoa dos Patos, Rio
745 Grande, RS. Dissertation, University of Rio Grande, Rio Grande do Sul, Brasil

746 Liu Q, Charette MA, Breier CF (2017) Geochimica et Cosmochimica Acta.
747 https://doi.org/10.1016/j.gca.2017.01.041

748 Maher DT, Eyre BD (2012) Carbon budgets for three autotrophic Australian estuaries:
749 Implications for global estimates of the coastal air-water CO_2 flux. Global
750 biogeochemical cycles. https://doi.org/10.1029/2011GB004075

751 Marques, WC (2012) The temporal variability of the freshwater discharge and water
752 levels at the Patos Lagoon, Brazil. International Journal of Geosciences.
753 https://doi.org/10.4236/ijg.2012.34076

754 Marques WC, Fernandes EH, Monteiro IO, Möller OO (2009) Numerical modeling of
755 the Patos Lagoon coastal plume, Brazil. Continental Shelf Research. 29:556–571

756 Marques WC, Möller OO (2008) Variabilidade temporal em longo período da descarga
757 fluvial e níveis de água da Lagoa dos Patos, Rio Grande do Sul, Brasil. Revista Brasileira
758 de Recursos Hídricos. 13: 155–163

759 Mendes CRB, Odebrecht C, Tavano VM, Abreu PC (2016) Pigment-based
760 chemotaxonomy of phytoplankton in the Patos Lagoon estuary (Brazil) and adjacente
761 coast. Marine Biology Research. https://doi.org/10.1080/17451000.2016.1189082

762 Millero FJ (2013) Chemical Oceanography. CRC Press.

763 Millero FJ, Graham TB, Huang F et al (2006) Dissociation Constants of Carbonic Acid
764 in Seawater as a Function of Salinity and Temperature. Marine Chemistry.
765 https://doi.org/10.1016/j.marchem.2005.12.001

766 Mirlean N, Calliari L, Johannesson K (2020) Dredging in an estuary causes contamination
767 by fluid mud on a tourist ocean beach. Evidence via REE ratios. Marine Pollution
768 Bulletin. https://doi.org/10.1016/j.marpolbul.2020.111495

769 Mirlean N, Calliari L, Johannesson K (2021) Reply to MPB-D-20-01629. Carlos Alberto
770 Eiras Garcia Heitor Evangelista Osmar Olinto Möller Jr.Comments on -Dredging in an
771 estuary causes contamination by fluid mud on a tourist oceanbeach. Evidence via REE
772 ratios- by N. Mirlean, L. Calliari, and K. Johannesson in Marine Pollution Bulletin 159
773 (2020) 111495. Marine Pollution Bulletin.
774 https://doi.org/10.1016/j.marpolbul.2021.112161

775 Möller OO, Castaing P, Salomon JC, Lazure P (2001) The Influence of Local and Non-
776 Local Forcing Effects on the Subtidal Circulation of Patos Lagoon. Estuaries. 24:297–
777 311

778 Möller OO, Fernandes EH (2010) Hidrologia e Hidrodinâmica. In: Seeliger, U. and
779 Odebrecht, C. (Eds.) O Estuário da Lagoa dos Patos: Um século de transformações. Rio
780 Grande, FURG, pp: 17–30.

781 Monteiro T, Kerr R, Orselli IBM, Lencina-Avila JM (2020) Towards an intensified
782 summer CO2 sink behaviour in the Southern Ocean coastal regions. Progress in
783 Oceanography. https://doi.org/10.1016/j.pocean.2020.102267

784 Moreau S, Penna AD, Llort J et al (2017) Eddy-induced carbon transport across the
785 Antarctic circumpolar current. Global Biogeochemical Cycles.
786 https://doi.org/10.1002/2017GB005669

787 Niencheski LF, Baumgarten MGZ, Cabrera L, Juliano SK (2006) Patos Lagoon:
788 indicators of organic pollution. Journal of Coastal Research. 39:1357–1359

789 Niencheski LF, Windom, HL (1994) Nutrient flux and budget in Patos Lagoon estuary.
790 Science of the Total Environment. https://doi.org/10.1016/0048-9697(94)90004-3

791 Noriega C, Araujo M (2014) Carbon dioxide emissions from estuaries of nothern and
792 northeastern Brazil. Scientific Reports. https://doi.org/10.1038/srep06164

793 Noriega CED, Araujo M, Lefèvre N (2013) Spatial and temporal variability of the CO_2
794 fluxes in a tropical, highly urbanized estuary. Estuaries and coast.
795 https://doi.org/10.1007/s12237-013-9608-1

796 Odebrecht C, Abreu PCOV (2019) Phytoplankton and water quality parameters in the
797 Patos Lagoon estuary and adjacent marine coast. Sistema de Informação sobre a
798 Biodiversidade Brasileira - SiBBr. Sampling event
799 dataset https://doi.org/10.15468/xmlvxm accessed via GBIF.org on 2020-06-09

800 Odebrecht C, Secchi ER, Abreu PC, Muelbert JH, Uiblein F (2017) Biota of the Patos
801 Lagoon estuary and adjacente marine coast: long-term changes induced by natural and
802 human-related factors. Marine Biology Research.
803 https://doi.org/10.1080/17451000.2016.1258714

804 Oliveira AP, Cabeçadas G, Mateus MD (2017) Inorganic carbon distribution and
805 CO_2 fluxes in a large European estuary (Tagus, Portugal). Scientific
806 Reports. https://doi.org/10.1038/s41598-017-06758-z

807 Orr JC, Epitalon J, Dickson AG, Gattuso J (2018) Routine uncertainty propagation for
808 the marine carbon dioxide system. Marine Chemistry.
809 https://doi.org/10.1016/j.marchem.2018.10.006

810 Pierrot D, Lewis E, Wallace DWR (2006) MS Excel Program Developed for CO_2 System
811 Calculations, ORNL/CDIAC-105a. Carbon Dioxide Information Analysis Center. Oak
812 Ridge National Laboratory, U.S. Department of Energy, Oak Ridge, Tennessee.
813 https://doi.org/10.3334/CDIAC/otg.CO2SYS_XLS_CDIAC105a

814 Raymond PA, Cole JJ (2001) Gas exchange in rivers and estuaries: Choosing a gas
815 transfer velocity. Estuaries. 24:312–317

816 Sadat-Noori M, Maher DT, Santos IR (2016) Groundwater discharge as a source of
817 dissolved carbon and greenhouse gases in a subtropical estuary. Estuaries and coasts.
818 https://doi.org/10.1007/s12237-015-0042-4

819 Sarma VVSS, Kumar MD, Manerikar M (2001) Emission of carbono dioxide from a
820 Tropical Estuarine System, Goa, India. Hydrology and Biogeochemical Cycles.
821 https://doi.org/10.1029/2000GL006114

822 Sarmiento J, Gruber N (2006) Ocean Biogeochemical Dynamics Princeton Univ. Press,
823 New Jersey.

824 Seeliger U, Odebrecht C (2010) O Estuário da Lagoa dos Patos: Um Século de
825 Transformações. Rio Grande, FURG.

826 Sims RP, Bedington M, Schuster U et al (2021) Tidal mixing of estuarine and coastal
827 waters in the Western English Channel controls spatial and temporal variability in
828 seawater CO_2, Biogeosciences Discuss. [preprint]. https://doi.org/10.5194/bg-2021-166

829 Sunda WG, Cai W (2012) Eutrophication induced CO_2–acidification of subsurface
830 coastal waters: interactive of temperature, salinity and atmospheric pCO2. Environmental
831 Science & Technollogy. https://doi.org/10.1021/es300626f

832 Takahashi T, Sutherland SC, Chipman DW (2014) Climatological distributions of pH,
833 pCO_2, total CO_2, alkalinity, and $CaCO_3$ saturation in the global surface ocean, and
834 temporal changes at selected locations Marine Chemistry.
835 https://doi.org/10.1016/j.marchem.2014.06.004

836 Takahashi T, Sutherland SC, Wanninkhof R et al (2009) Climatological mean and decadal
837 change in surface ocean pCO_2, and net sea-air CO_2 flux over the global oceans. Deep sea
838 research part II: Topical studies in oceanography.
839 https://doi.org/0.1016/j.dsr2.2008.12.009

840 Thoning KW, Crotwell AM, Mund JW (2021) Atmospheric carbon dioxide dry air mole
841 fractions from continuous measurements at Mauna Loa, Hawaii, Barrow, Alaska,
842 American Samoa and South Pole. 1973-2020, Version 2021-08-09 National Oceanic and
843 Atmospheric Administration (NOAA), Global Monitoring Laboratory (GML), Boulder,
844 Colorado, USA https://doi.org/10.15138/yaf1-bk21 FTP path:
845 ftp://aftp.cmdl.noaa.gov/data/greenhouse_gases/co2/in-situ/surface/

846 Torres JR, Philomena LA (2013) Environmental Port Management: Conceptual Model
847 Development and Use of Tools to Evaluate and Monitor Dredging Activities in the Port
848 of Rio Grande, Brazil. African Journal of Environmental Economic and Management.
849 1:22–27

850 Uppström LR (1974) Boron/chlorinity ratio of deep-sea water from the Pacific Ocean.
851 Deep-Sea Res. 21:161–162

852 Van Dam BR, Crosswell JR, Paerl HW (2018) Flood-driven CO2 emissions from
853 adjacent North Carolina estuaries during Hurricane Joaquim (2015). Marine Chemistry.
854 https://doi.org/10.1016/j.marchem.2018.10.001

855 Vaz AC, Möller OO, Almeida TL (2006) Análise quantitativa da descarga dos rios
856 afluentes da Lagoa dos Patos. Atlântica. 28:13–23

857 Wallner-Kersanach M, Mirlean N, Baumgarten MGZ et al (2016) Temporal evolution of
858 the contamination in the southern area of the Patos Lagoon estuary, RS, Brazil. Journal
859 of Integrated Coastal Zone Management. https://doi.org/10.5894/rgci596

860 Wanninkhof R (2014) Relationship between wind speed and gas exchange over the ocean
861 revisited. Limnology and oceanography. https://doi.org/10.4319/lom.2014.12.351

862 Weiss RF (1974) Carbon dioxide in water and seawater: the solubility of a non-ideal gas.
863 Marine Chemistry. https://doi.org/10.1016/0304-4203(74)90015-2

Weiss RF, Price BA (1980) Nitrous oxide solubility in water and seawater. Marine Chemistry. https://doi.org/10.1016/0304-4203(80)90024-9

Yao H, Hu X (2017) Responses of carbonate system and CO_2 flux to extended drought and intense flooding in a semiarid subtropical estuary. Limnology and Oceanography. https://doi.org/10.1002/lno.10646

Yao H, McCutcheon MR, Staryk CJ, Hu X (2020) Hydrologic controls on CO_2 chemistry and flux in subtropical lagoonal estuaries of the northwestern Gulf of Mexico. Limnology and Oceanography. https://doi.org/10.1002/lno.11394

Statements & Declarations

The authors declare that they have no known competing financial interests or personal relationships that could have appeared to influence the work reported in this paper.

Supplementary Files

This is a list of supplementary files associated with this preprint. Click to download.

- Albuquerqueetal2SupplementaryMaterial.docx